

# There and back again: outspiralling motion in non-Kerr compact objects

Manuel O. Mariano<sup>1</sup> and C. A. R. Herdeiro<sup>1,2</sup>

<sup>1</sup>Departamento de Matemática da Universidade de Aveiro and Center for Research and Development in Mathematics and Applications – CIDMA Campus de Santiago, 3810-183 Aveiro, Portugal

<sup>2</sup>Programa de Pós-Graduação em Física, Universidade Federal do Pará, 66075-110, Belém, Pará, Brazil

July 2025

## Abstract

In Keplerian dynamics, a test body orbiting a point particle in circular motion has a monotonically increasing frequency, with decreasing radius. If a dissipative channel is introduced, such as gravitational wave (GW) emission, (say) under the quadrupole approximation, the corresponding GW strain has an ever increasing frequency with time. A similar statement holds for equatorial motion of a test particle on the Kerr manifold, except such inspiral is cut off at the ISCO, wherein stable circular orbits cease to exist and a plunge is expected. We analyse circular timelike orbits in generic spinning spacetimes and study the conditions in which *exotic* motion can occur, due to the presence of non-Kerr features. In particular, we derive conditions under which an inspiral towards a compact object is naturally followed by an *outspiral* motion, and give concrete examples, as well as the corresponding GW phenomenology. This analysis serves both as a theoretical exploration of non-Kerrness as well as an example of a concrete smoking gun of exotic spacetimes.

## Contents

<b>1</b>	<b>Introduction</b>	<b>2</b>
<b>2</b>	<b>Circular orbits in generic rotating spacetimes</b>	<b>2</b>
2.1	The case of Kerr . . . . .	4
<b>3</b>	<b>Evolution between circular orbits</b>	<b>5</b>
3.1	Adiabatic energy emission - Quadrupole waves . . . . .	5
3.2	Critical points of $dR/dt$ . . . . .	6
3.3	Duration of the inspiral and outcome of the outspiral . . . . .	8
<b>4</b>	<b>The quasi-circular outspiralling - concrete illustrations</b>	<b>8</b>
4.1	Engineered geometry . . . . .	9
4.2	Spinning boson stars . . . . .	9
<b>5</b>	<b>Gravitational Wave Signatures</b>	<b>11</b>
5.1	Engineered example . . . . .	11
5.2	Spinning boson stars . . . . .	12
<b>6</b>	<b>Conclusions and Discussions</b>	<b>13</b>
<b>7</b>	<b>Acknowledgements</b>	<b>14</b>
	<b>References</b>	<b>14</b>

arXiv:2507.19582v1 [gr-qc] 25 Jul 2025

# 1 Introduction

The detection of  $\mathcal{O}(100)$  Gravitational Waves (GWs) events by the LIGO/Virgo/KAGRA collaboration [1–4] from the coalescence of stellar mass black holes (BHs) and neutron stars, has allowed for unprecedented tests of general gravity (GR) in the strong field regime [5]. In the future, space-based detectors such as the Laser Interferometer Space Antenna (LISA) [6], will be observing GWs from supermassive BH mergers and highly asymmetric binaries, which will allow probing GR against novel astrophysical phenomena [7–10].

Anchored on well-established uniqueness theorems [11–13], GR suggests that all isolated astrophysical BH candidates, ranging (at least) 10 orders of magnitude in mass, are described by the Kerr solution. This is the *Kerr Hypothesis*. Stable (on cosmological timescales) non-Kerr models with a plausible dynamical formation mechanism, however, can emerge naturally from minimally coupled GR to exotic matter or modified gravity theories [14], and challenge this hypothesis. Thus, it is crucial to explore and model smoking gun non-Kerr features of these objects, to then search for them in the detected GW signals [15].

The study of spacetime geodesics can play an important role in searching for non-Kerr signatures. In a metric theory of gravity, the orbits of a light compact object (LCO) around a massive compact object (MCO), with a much larger mass, are adequately described by geodesics of the MCO’s spacetime. The geodesic structure for both Kerr [16, 17] and a variety of non-Kerr spacetimes [18–33] has been extensively studied in the literature. Examples of non-Kerr *qualitative* geodesic features are: the occurrence of pointy-petal orbits and semi-orbits [19, 20, 34], static rings (SRs) and light points [34, 35], disconnected regions of timelike stable circular orbits [24, 30] or even chaotic signatures due to non-integrable geodesics [25, 36]. These non-Kerr attributes may leave detectable phenomenological imprints [23, 29, 30, 37–43], for instance in the emitted gravitational waveform. Radiated GWs will carry energy away from the binary, making the LCO move in a “quasi-geodesic” motion. Under the *adiabatic approximation* [44–47] a two-timescale approach is employed, whereby the LCO moves along geodesics with a constant orbital energy at timescales of the orbital period, only inspiralling inwards for much larger times. Although this approximation neglects backreacting self-force terms [48], it is commonly assumed in the study of extreme mass ratio inspirals (EMRIs), one of LISA’s key targets [49–52].

A particular example of a non-Kerr GW signature was found in [23] and [38], where equatorial quasi-circular EMRIs around Kerr BHs with scalar hair were studied. These are composite spinning horizon-boson star systems, that emerge as solutions of the Einstein-(complex)-Klein-Gordon theory [53–55]. They can form dynamically through the superradiant instability [56–58], provided that (in  $G = c = 1$  units) the Compton wavelength  $1/\mu$  of the scalar field, with  $\mu$  the boson’s mass, is larger than the horizon scale set by the BH mass  $\mathcal{M}$ , i.e.,  $\mathcal{M}\mu \leq 1$ . For some very hairy solutions, it was found that the GW signal can backward chirp, due to the non-monotonicity of the metric functions for such spacetimes [59].

For a Kerr BH MCO, as the LCO radiates GWs in an equatorial quasi-circular motion, it will transition to circular geodesics with lower radii, until the innermost stable circular orbit (ISCO) is reached, wherein the LCO plunges. In [60], it was claimed that adiabatic loss of energy always causes the LCO to slowly inspiral towards the MCO, ending either in a plunge (just like in Kerr) or on a SR that coincides with a minima of the generalized Newtonian potential. In this work, we claim that an extra possibility should also be considered. It is possible for the LCO to reach an orbit where prograde and retrograde motions become degenerate, and energy loss leads to a continuous *transition from an inspiralling to an outspiralling regime*. Moreover, this non-Kerr feature can be found in rotating spacetimes with non-monotonic behaviour of the metric functions. This can be realized, for instance, in off-centered mass distributions. Two concrete families of examples are discussed below.

This work is organized as follows. In section 2, we discuss equatorial circular geodesics for a generic  $\mathbb{Z}_2$ , asymptotically flat, circular and rotating spacetime. In section 3, we consider an energy loss mechanism, via the emission of GWs under the quadrupole approximation, and set the conditions under which an outspiral motion is possible, determining also its possible outcomes. In section 4 we describe spacetimes where the outspiral is possible, and in section 5 we discuss the GW signatures of this regime on such spacetimes.

## 2 Circular orbits in generic rotating spacetimes

Consider a compact object, with or without an event horizon, which is stationary, axi-symmetric and asymptotically flat, in 1+3 dimensions. The two Killing vector fields  $\chi^\mu$  and  $\eta^\mu$  are associated, respectively, with stationarity and axi-symmetry. Then, it holds that  $[\chi, \eta] = 0$  [61]. Therefore, a coordinate system  $(t, r, \theta, \varphi)$  adapted simultaneously to both symmetries exists;  $\chi = \partial_t$  and  $\eta = \partial_\varphi$ . Moreover, the spacetime is assumed circular:  $\chi^\mu R_\mu^{[\nu} \chi^\rho \eta^{\sigma]} = \eta^\mu R_\mu^{[\nu} \chi^\rho \eta^{\sigma]} = 0$ , where  $R_{\mu\nu}$  is the Ricci tensor. Physically, this means there are only energy currents along  $\partial_\varphi$ , but not convective ones along the meridional planes [60] or radial ones. For asymptotically flat spacetimes, circularity

implies that the 2-planes orthogonal to  $\eta^\mu$  and  $\chi^\mu$  are integrable, i.e span a 2-surface [62]. Therefore, one can set the coordinates  $(r, \theta)$  to parameterize the orthogonal 2-surface, as well as orthogonal amongst themselves [17]. This yields the metric [24]

$$ds^2 = g_{tt}(r, \theta)dt^2 + 2g_{t\varphi}(r, \theta)dtd\varphi + g_{\varphi\varphi}(r, \theta)d\varphi^2 + g_{rr}(r, \theta)dr^2 + g_{\theta\theta}(r, \theta)d\theta^2. \quad (1)$$

Observe that circularity implies the discrete symmetry  $(t, \varphi) \rightarrow (-t, -\varphi)$ . Gauge freedom allows to set the event horizon, if it exists, at a constant (positive) radial coordinate  $r = r_H$ . Thus, the exterior spacetime is  $r_H < r < \infty$  (or  $0 \leq r < \infty$  if no horizon exists). Asymptotically (at  $r \rightarrow \infty$ ) our coordinates must match the standard spherical coordinates. Thus, the standard coordinate ranges  $\theta \in [0, \pi]$ ,  $\varphi \in [0, 2\pi[$  and  $t \in ]-\infty, +\infty[$  apply. Finally, a  $\mathbb{Z}_2$  symmetry,  $\theta \rightarrow \pi - \theta$  is imposed, defining an ‘‘equator’’ at  $\theta = \pi/2$  as its set of fixed points. This is a totally geodesic sub-manifold. On this equator, the perimetral radius  $R = \sqrt{g_{\varphi\varphi}}|_{\theta=\pi/2}$  is used,<sup>1</sup> such that the integral lines of  $\partial_\varphi$  are circumferences with perimeter  $2\pi R$ . Therefore, the equatorial plane metric becomes

$$ds_{\theta=\pi/2}^2 = g_{tt}(R, \pi/2)dt^2 + 2g_{t\varphi}(R, \pi/2)dtd\varphi + R^2d\varphi^2 + g_{RR}(R, \pi/2)dR^2. \quad (2)$$

Consider now circular equatorial timelike geodesics in this spacetime. The equations of motion for a timelike geodesic can be obtained from the following Lagrangian  $\mathcal{L}$

$$\frac{2\mathcal{L}}{m} = g_{\mu\nu}\dot{x}^\mu\dot{x}^\nu = g_{tt}\dot{t}^2 + 2g_{t\varphi}\dot{t}\dot{\varphi} + R^2\dot{\varphi}^2 + g_{RR}\dot{R}^2 = -1, \quad (3)$$

where the dot stands for a derivative with respect to the proper time  $\tau$  and  $m$  for the LCO’s mass. To each Killing vector is associated a constant of motion

$$E = -g_{\mu\nu}\dot{x}^\mu\chi^\nu = -g_{tt}\dot{t} - g_{t\varphi}\dot{\varphi}, \quad (4)$$

$$L = g_{\mu\nu}\dot{x}^\mu\eta^\nu = g_{t\varphi}\dot{t} + R^2\dot{\varphi}. \quad (5)$$

These quantities are, respectively, the energy and angular momentum per unit mass of the LCO. Plugging eqs. (4) and (5) into the Lagrangian in eq. (3), we get,

$$g_{RR}\dot{R}^2 = -1 + \frac{R^2E^2 + 2g_{t\varphi}EL + g_{tt}L^2}{B(R)} \equiv V(R, E, L), \quad (6)$$

where

$$B(R) \equiv g_{t\varphi}^2 - g_{tt}R^2. \quad (7)$$

The problem has been reduced to a particle moving in a 1D effective potential  $V$ , with  $g_{RR}$  acting as a position-dependent mass term. In the domain of outer communications  $B(R) > 0$  due to the signature of the metric in the  $(t, \varphi)$  sector.

A generic equatorial orbit requires solving eqs. (4) to (6), 3 differential equations for the 3 unknown functions  $t(\tau), \varphi(\tau), R(\tau)$ , with  $E$  and  $L$  constant. For the *special case* of circular orbits,  $R = R_{\text{circ}} = \text{const.}$ , however, eq. (6) trivializes

$$V(R_{\text{cir}}, E, L) = 0, \quad (8)$$

which yields multiple circular worldlines as solutions. To obtain  $R = R(E, L)$  of the unique geodesic worldline, a further condition must be used [63]. This is provided using the standard Euler-Lagrange equation for  $R$  from eq. (3), leading to

$$\left(\frac{dV}{dR}\right)_{R=R_{\text{cir}}} \equiv V'(R_{\text{cir}}, E, L) = 0. \quad (9)$$

To further impose that the circular orbit at  $R = R_{\text{cir}}$  is stable, one must ensure, additionally

$$\left(\frac{d^2V}{dR^2}\right)_{R=R_{\text{cir}}} \equiv V''(R_{\text{cir}}, E, L) < 0. \quad (10)$$

Together with eq. (6), that defines  $V$ , eqs. (8) and (9) yield  $E$  and  $L$  for circular orbits. Due to the quadratic nature of the equations, one obtains a pair of solutions corresponding to prograde (labelled  $+$ ) and retrograde (labelled  $-$ ) orbits. As we will later see, retrograde (prograde) *does not mean* co-rotating (counter-rotating) relative to the MCO; retrograde (prograde) orbits can be co-rotating (counter-rotating), and have positive (negative) angular

<sup>1</sup>Outside the horizon, causality requires that  $g_{\varphi\varphi} \geq 0$ .

momentum, with the MCO also having a positive angular momentum. Prograde (retrograde) only matches co-rotation (counter-rotation) sufficiently far away from the the MCO.

To write the solutions, it is useful to introduce the angular velocity of the LCO,

$$\Omega \equiv \frac{d\varphi}{dt} = \frac{\dot{\varphi}}{\dot{t}} = -\frac{Eg_{t\varphi} - Lg_{tt}}{ER^2 + Lg_{t\varphi}}, \quad (11)$$

where from now on we drop the subscript “cir” in  $R_{\text{cir}}$  but it is understood this refers to the radius of a timelike, circular equatorial orbit. The solution can be written as

$$E_{\pm} = -\frac{g_{tt} + g_{t\varphi}\Omega_{\pm}}{\sqrt{\beta_{\pm}}}, \quad (12)$$

$$L_{\pm} = \frac{g_{t\varphi} + R^2\Omega_{\pm}}{\sqrt{\beta_{\pm}}}, \quad (13)$$

$$\Omega_{\pm} = \frac{-g'_{t\varphi} \pm \sqrt{C}}{2R}, \quad (14)$$

where we have defined

$$C \equiv (g'_{t\varphi})^2 - 2g'_{tt}R, \quad (15)$$

and

$$\beta_{\pm} \equiv -g_{tt} - 2g_{t\varphi}\Omega_{\pm} - R^2\Omega_{\pm}^2. \quad (16)$$

For timelike circular orbits, we must have  $C \geq 0$  and  $\beta_{\pm} > 0$ . Below, we will mention what occurs when these inequalities break down. For now, observe that, at the radius where  $C = 0$ ,  $\Omega_+ = \Omega_-$  and so there is a degeneracy between prograde and retrograde orbits, implying only one possible circular geodesic motion. Finally, one can also express the second derivative of the potential as

$$V''_{\pm} = \frac{\Omega_{\pm}^2 \gamma_{\varphi\varphi} + 2\Omega_{\pm} \gamma_{t\varphi} + \gamma_{tt}}{B\beta_{\pm}}, \quad (17)$$

with

$$\gamma_{\mu\nu} = g''_{\mu\nu}B + 2g_{\mu\nu}C. \quad (18)$$

## 2.1 The case of Kerr

To provide some intuition, we will now specify some of the above quantities in the case of Kerr. In Boyer-Lindquist (BL) coordinates  $(t, r, \theta, \varphi)$ , the Kerr metric takes the form

$$ds^2 = -\frac{\Delta}{\Sigma} (dt - a \sin^2 \theta d\varphi)^2 + \frac{\Sigma}{\Delta} dr^2 + \Sigma d\theta^2 + \frac{\sin^2 \theta}{\Sigma} [adt - (r^2 + a^2)d\varphi]^2, \quad (19)$$

with  $\Sigma \equiv r^2 + a^2 \cos^2 \theta$  and  $\Delta \equiv r^2 - 2Mr + a^2$ . The metric is described by two macroscopic parameters, the mass  $M$  and the angular momentum  $J = aM$ . It is more instructive, however, to write the metric in coordinates where  $r \rightarrow \tilde{r} \equiv r/M$ . In this case, the metric components depend uniquely on the dimensionless parameter  $j \equiv J/M^2$ , up to multiplicative factors of  $M$ . To avoid a naked singularity, the Kerr bound must be obeyed  $0 \leq j \leq 1$ . Focusing on the equatorial plane alone ( $\theta = \pi/2$ ), one obtains that

$$\widetilde{g}_{tt} \equiv g_{tt} = 1 - \frac{2}{\tilde{r}}, \quad (20)$$

$$\widetilde{g}_{t\varphi} \equiv g_{t\varphi}/M = -\frac{2j}{\tilde{r}}, \quad (21)$$

$$\widetilde{g}_{\varphi\varphi} \equiv g_{\varphi\varphi}/M^2 \equiv \tilde{R}^2 = \tilde{r}^2 + j^2 \left(1 + \frac{2}{\tilde{r}}\right), \quad (22)$$

with  $\tilde{R} \equiv R/M$  the dimensionless perimetral radius and where the metric components with a tilde are also dimensionless. The relevant functions for equatorial, circular geodesics on the Kerr spacetime can be determined by using eqs. (20) to (22) on eqs. (12) to (17), yielding

$$C = \frac{4}{\tilde{r}}, \quad (23)$$

$$M\Omega_{\pm} = \frac{1}{j \pm \tilde{r}^{3/2}}, \quad (24)$$

$$\beta_{\pm} = \frac{(\tilde{r} - 3)\tilde{r}^2 \pm 2j\tilde{r}^{3/2}}{(j \pm \tilde{r}^{3/2})^2}, \quad (25)$$

$$E_{\pm} = \frac{(\tilde{r} - 2)\tilde{r} \pm j\sqrt{\tilde{r}}}{\tilde{r}\sqrt{(\tilde{r} - 3)\tilde{r} \pm 2j\sqrt{\tilde{r}}}}, \quad (26)$$

$$L_{\pm} = \pm \frac{\tilde{r}^2 \mp 2j\sqrt{\tilde{r}} + j^2}{\sqrt{\tilde{r} [(\tilde{r} - 3)\tilde{r} \pm 2j\sqrt{\tilde{r}}]}}, \quad (27)$$

$$V_{\pm}'' = \frac{2 [3j^2 \mp 8j\sqrt{\tilde{r}} + (6 - \tilde{r})\tilde{r}]}{[\pm 2j\tilde{r}^{3/2} + (\tilde{r} - 3)\tilde{r}^2] [(\tilde{r} - 2)\tilde{r} + j^2]}. \quad (28)$$

The results are written in terms of the dimensionless radial BL coordinate  $\tilde{r}$ . To convert  $\tilde{r}$  to the dimensionless perimetral radius, one must solve the cubic equation from eq. (22). Using Viète's solution [64], and choosing the solution that matches  $\tilde{r} = \tilde{R}$  when  $j = 0$ , one finds that

$$\tilde{r} = 2\sqrt{\frac{\tilde{R}^2 - j^2}{3}} \cos\left(\frac{1}{3} \arccos\left[\sqrt{\frac{27}{(\tilde{R}^2 - j^2)^3}} j^2\right]\right). \quad (29)$$

In the limit  $R \gg 1$ , the two radii also coincide. Moreover, at the outer horizon, where  $\tilde{r}_H = 1 + \sqrt{1 - j^2}$ , one obtains that  $\tilde{R}_H = 2$  independently of the value of  $j$ .

From the above equations it follows that  $C$  and  $\Omega_{\pm}$  have no zeros; on the other hand,  $\beta_{\pm}$  and  $V_{\pm}''$  have zeros. In the limit  $j = 0$ , these are, respectively, at  $\tilde{r} = 3$  and  $\tilde{r} = 6$ , which one identifies as the light ring (LR) and ISCO in Schwarzschild. As we shall see below, the zeros of these quantities are significant for the geodesic motion for generic spacetimes under the conditions specified in section 2.

### 3 Evolution between circular orbits

#### 3.1 Adiabatic energy emission - Quadrupole waves

Let us consider an energy dissipation mechanism allowing the LCO to evolve between timelike equatorial circular orbits. When the radiated energy during one orbit is much smaller than the orbital energy of the LCO, and thus the orbital period will be much shorter than the timescale of the inspiral,  $T_{\text{inspiral}} \gg T_{\text{orbit}}$ , an adiabatic approximation holds. Then, the LCO motion can be approximated as a sequence of equatorial geodesics, with the energy and angular momentum fluxes (per unit mass),  $dE/dt$  and  $dL/dt$  respectively, dictating the transitions. Moreover, if the LCO follows a circular geodesic it will progress to another circular geodesic, following a quasi-circular motion, provided the fluxes obey

$$\frac{dL}{dt} = \frac{1}{\Omega} \frac{dE}{dt}. \quad (30)$$

The backreaction from radiative mechanisms, such as gravitational or electromagnetic radiation, obey eq. (30), while environmental effects, such as accretion or dynamical friction, may, in general, lead to an increase of the orbital eccentricity [65]. Here, we shall consider the former only.

For quasi-circular motion, dissipated energy  $\delta E < 0$  leads to an adiabatic shift in the orbital radius  $\delta R$ :

$$\delta E = E' \delta R \Rightarrow \frac{dE}{dt} = E' \frac{dR}{dt}. \quad (31)$$

By differentiating eq. (12), one arrives at [38, 60]

$$E'_{\pm} = \mp \frac{B\Omega_{\pm} V_{\pm}''}{2\sqrt{\beta_{\pm} C}}. \quad (32)$$

Consider GW emission, modelled by the quadrupole approximation, as the energy dissipation mechanism. Let the dissipated energy be normalized to the mass of the LCO, to match the orbital definition. Then, the radiated energy (per unit mass) flux is

$$\frac{dE}{dt} = -\frac{1}{5m} \left\langle \frac{d^3 J_{ij}}{dt^3} \frac{d^3 J_{ij}}{dt^3} \right\rangle, \quad (33)$$

with  $J_{ij} = I_{ij} - \frac{1}{3}\delta^{ij}I_{ij}$ , the reduced quadrupole moment and

$$I_{ij} = \int y_i y_j \rho(t, \vec{y}) d^3 y, \quad (34)$$

where  $\rho(t, \vec{y})$  is the energy density. Treating both the LCO and the MCO as point-like masses, with the MCO fixed at the origin and  $\vec{y}_{\text{LCO}} = (R \cos \Omega t, R \sin \Omega t, 0)$ , yields

$$\rho(t, \vec{y}) = m \delta^{(3)}(\vec{y} - \vec{y}_{\text{LCO}}). \quad (35)$$

The MCO contribution for  $\rho$  was not included, as its position is fixed at the origin. The energy (per unit mass) flux thus becomes

$$\frac{dE}{dt} = -\frac{32}{5} m R^4 \Omega^6, \quad (36)$$

with the angular momentum flux obeying eq. (30).

From eqs. (32) and (36), the LCO's radial coordinate evolution due to GWs emission reads [38]

$$\frac{dR}{dt} = \pm \frac{64}{5} m R^4 \Omega_{\pm}^5 \frac{\sqrt{\beta_{\pm} C}}{B V_{\pm}''}. \quad (37)$$

Alternatively, using eq. (17), this can also be expressed as

$$\frac{dR}{dt} = \pm \frac{64}{5} m R^4 \Omega_{\pm}^5 \frac{\beta_{\pm}^{3/2} C^{1/2}}{\Omega_{\pm}^2 \gamma_{\varphi\varphi} + 2\Omega_{\pm} \gamma_{t\varphi} + \gamma_{tt}}. \quad (38)$$

### 3.2 Critical points of $dR/dt$

Inspection of (37) and (38) reveals that the behaviour of  $dR/dt$  has critical points at zeros of the functions  $\Omega_{\pm}$ ,  $V_{\pm}''$ ,  $\beta_{\pm}$  and  $C$ . To contextualize, for equatorial circular orbits [24], the following meanings apply:

$$V'' < 0 \quad (\text{Stability condition}) \quad (39)$$

$$\beta_{\pm} > 0 \quad (\text{Timelike condition}) \quad (40)$$

$$C > 0 \quad (\text{Existence condition}). \quad (41)$$

In the far region (from the MCO), Keplerian mechanics, and thus all these three conditions, must hold. Then, it is expected that as energy is lost via emission of gravitational waves, the object will transition to orbits with progressively lower radii. This is confirmed, e.g., from eq. (37). Indeed, prograde (retrograde) orbits obey  $\Omega_+ > 0$  ( $\Omega_- < 0$ ). Thus, considering (39), in the far away region one gets  $dR/dt < 0$  in both cases.

In the near region, however, such behaviour may end. The LCO may reach a last stable circular orbit continuously connected to spatial infinity. This is dubbed *marginally stable circular orbit* (MSCO). For Kerr BHs, it coincides with the ISCO. In more generic compact objects, however, this needs not be the case, and the specific behaviour depends on the type of critical point for  $dR/dt$ , which we split into four distinct groups [24, 38].

- $V_{\pm}'' = 0$ : eq. (37) predicts that  $dR/dt \rightarrow +\infty$  and thus a breakdown of the adiabaticity condition. Physically, this corresponds to the end of the *stable* circular orbits region. Then, the LCO will enter a *transition* regime. This may connect the inspiral and the plunge towards the MCO, as in Kerr. But in other compact objects, one could envisage different possibilities, as other, more interior, disconnected regions with stable timelike circular orbits could exist [24, 30].
- $\beta_{\pm} = 0$ : naively, the MSCO could be located at the outermost LR, determined by  $\beta_{\pm}(R_{\text{LR}}) = 0$  [24]. Then, eq. (37) would predict  $dR/dt \rightarrow 0$ . For a vast class of ultracompact objects, however, with or without an event horizon, the outermost LR will be unstable [38, 66, 67]. Timelike circular orbits in the vicinity of an unstable LR, are either unstable or non-existent [24]. Therefore, a larger radius where  $V_{\pm}'' = 0$  should exist, leading to the previous case.

- $\Omega_{\pm} = 0$ : this corresponds to a SR; with respect to an asymptotic static observer, an object following such an orbit would appear static. At the SR, the orbital energy simplifies to

$$(E_{\pm})_{\text{SR}} = \sqrt{(\beta_{\pm})_{\text{SR}}} = \sqrt{-g_{tt}}, \quad (42)$$

which corresponds to the local redshift factor. Thus a SR cannot occur inside an ergoregion. From eqs. (14) and (15)  $(g'_{tt})_{\text{SR}} = 0$ ; thus SRs occur at local extrema of  $g_{tt}$ . Moreover, a SR is stable if  $(g''_{tt})_{\text{SR}} < 0$ .<sup>2</sup> This could naturally occur in objects with an off-centered matter distribution, *e.g.* spinning boson stars (BSs) [34, 40], Proca stars [30] or Kerr BHs with scalar hair [38, 39]. Additionally, a SR coincides with a LR when  $g_{tt} = g'_{tt} = 0$ . Such orbits are dubbed *light points*, as photons would be at rest relative to an asymptotic observer [35].

As the LCO approaches a SR, eq. (37) predicts  $dR/dt \rightarrow 0$ . Thus, the SR represents the endpoint of the LCO inspiral evolution, acting as a *floating orbit* of this spacetime, due to the energy flux  $dE/dt \rightarrow 0$ . From eq. (32), the SR coincides with an extreme of the orbital energy. If it is a minimum, it acts as an accumulation point for infalling matter. Even if the LCO would be initially placed at a circular orbit below the SR, it would actually outspiral towards the SR [38, 60].

- $C = 0$ : if  $C(R_C) = 0$  and  $C(R) > 0$  for  $R > R_C$ , then as  $R \rightarrow R_C$ ,  $dR/dt \rightarrow 0$ , from eq. (37). Unlike the SR case, however, in this case  $dE/dt = 0$  is not guaranteed by (36), suggesting the evolution must continue rather than attaining a floating orbit. Indeed an interesting turn of affairs ensues.

From eqs. (12) to (16), at  $R = R_C$  the prograde and retrograde orbits become degenerate, allowing a *transition* between them. Assume, for concreteness  $\Omega_+ > 0$  at  $R = R_C$ ; a similar analysis holds for the other case. Then, from eq. (37), in the prograde case,  $dR/dt(R_C + \epsilon) < 0$ , ( $\epsilon > 0$ ) whereas in the retrograde case,  $dR/dt(R_C + \epsilon) > 0$ . Thus an LCO arriving at  $R_C$  in a prograde motion transitions to retrograde motion and *outspirals*. Indeed, from eq. (32), at  $R = R_C + \epsilon$ ,  $E'_+ > 0$  and  $E'_- < 0$ , so that energy can continue to be dissipated, as long as the LCO transitions from an inspiralling prograde orbit, to an outspiralling retrograde orbit, at  $R_C$  - see Fig. 1.

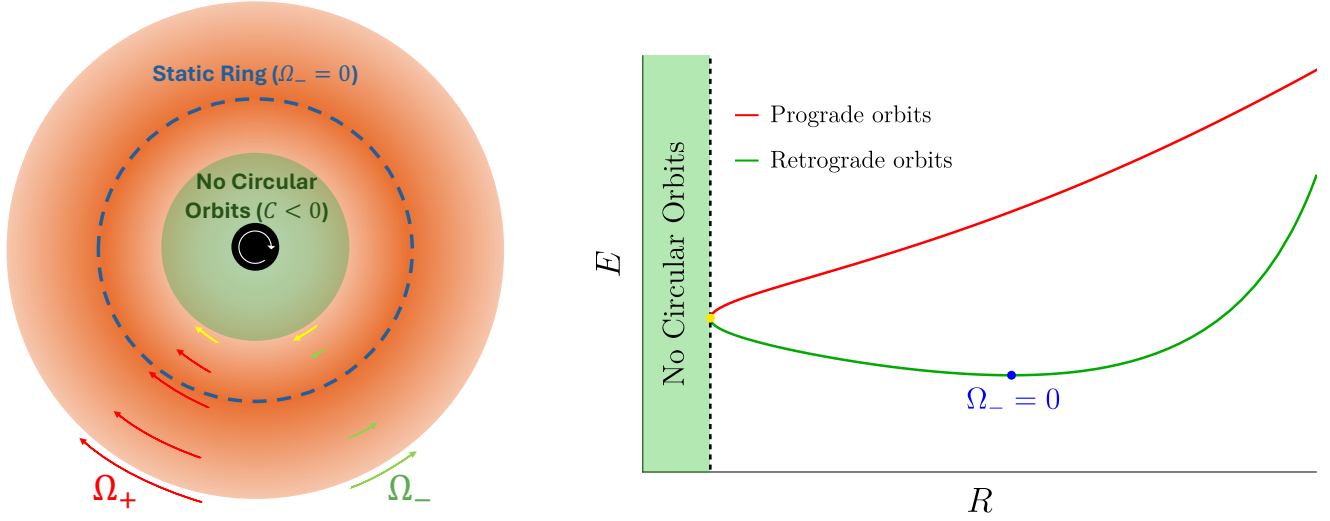


Figure 1: Illustration of the LCO motion with inspiral and outspiral. (Left) The spinning MCO is envisioned as a core (black) and a surrounding environment (orange). Darker tones represent regions with higher density. A central (green) region has no circular orbits and a static ring (blue dashed line) is assumed for retrograde orbits. The arrows in red (green) represent qualitatively the evolution of the angular velocity for prograde (retrograde) orbits  $\Omega_+$  ( $\Omega_-$ ), becoming degenerate at  $C = 0$ , (yellow arrows), where  $\Omega_+ = \Omega_-$ . (Right) Radial dependence of the circular orbits' energy. The yellow dot represents the radius at which  $C = 0$ , and  $E_+ = E_-$ . The LCO initially inspirals along prograde orbits, and then continues to lose energy by transitioning to a retrograde orbit at  $R_C$  outspiralling towards the SR.

<sup>2</sup>For spherically symmetric spacetimes, this condition is sufficient *and necessary* to ensure stability. In the rotating case, it is only sufficient.

### 3.3 Duration of the inspiral and outcome of the outspiral

The outspiral behavior just described raises two questions. Firstly, does the inspiral until  $R_C$  occur in a finite time? Secondly, assuming the outspiral occurs, what is the endpoint of the evolution?

Let us address the first question. One can calculate the time  $\Delta t$  taken to inspiral from an initial circular orbit at radius  $R_0 > R_C$ , along prograde orbits,<sup>3</sup> by evaluating

$$\Delta t = - \int_{R_C}^{R_0} \left[ \frac{64}{5} m r^4 \Omega_+^5 \frac{\beta_+^{3/2} C^{1/2}}{\Omega_+^2 \gamma_{\varphi\varphi} + 2\Omega_+ \gamma_{t\varphi} + \gamma_{tt}} \right]^{-1} dR \equiv - \int_{R_C}^{R_0} \frac{dR}{f(R)}, \quad (43)$$

where the function  $f(R)$  corresponds to the right hand side of eq. (37). At  $R_C$ ,  $f \rightarrow 0$ , and the convergence of eq. (43) needs to be studied with care. Expanding  $f$  around its zero  $R_C$ , using an ordinary Taylor series, leads to problems as  $f' \rightarrow +\infty$  at  $R_C$ . Yet, one can expand  $f^2$ , thus yielding

$$f(R) = \underbrace{\left( \frac{64}{5} m R^4 \Omega_+^5 \frac{\beta_+^{3/2}}{\Omega_+^2 \gamma_{\varphi\varphi} + 2\Omega_+ \gamma_{t\varphi} + \gamma_{tt}} \left( \frac{dC}{dR} \right)^{1/2} \right)}_{\equiv C_0} \Big|_{R=R_C} \sqrt{R - R_C} + \mathcal{O}(\sqrt[3]{R - R_C}). \quad (44)$$

For  $R < R_C$  ( $R > R_C$ ),  $C < 0$  ( $C > 0$ ); then  $dC/dR > 0$  at  $R_C$ . From this expansion, one can then decompose the integral into a sum of two terms

$$\Delta t = - \left( \int_{R_C+\epsilon}^{R_0} \frac{dR}{f(R)} + \frac{1}{C_0} \int_0^\epsilon \frac{d\epsilon'}{\sqrt{\epsilon'}} \right), \quad (45)$$

with  $\epsilon$  some arbitrarily small positive quantity, allowing us to disregard all higher order terms in the second term. From eq. (45), it is then clear that both pieces converge, and so *the LCO will reach  $R_C$  in a finite amount of time*, proceeding then to outspiral along retrograde orbits.

Consider now the second question: the possible endpoints of the outspiral regime. As  $\Omega_+ = \Omega_-$  at  $R = R_C$ , while near spatial infinity  $\Omega_- < 0$  and  $\Omega_+ > 0$ , there will always be a zero of either  $\Omega_+$  or  $\Omega_-$  between  $R_C$  and infinity. For concreteness, assume  $\Omega_-$  is the one vanishing. Similar considerations apply to the other case. Then, there are several possibilities:

- i) This zero of  $\Omega_-$  is a SR *and* it is continuously connected to  $R_C$  by stable timelike retrograde orbits. That is, conditions (39) and (40) both hold between  $R_C$  and  $R_{SR}$ . Then, the outspiral will end at the SR. Computing  $\Delta t$  for such outspiral between  $R_C$  and  $R_{SR}$ , considering that  $f \sim (R - R_{SR})^5$  in the SR's vicinity [38], one observes that *the LCO will reach the SR in an infinite amount of time*.<sup>4</sup> Globally, if (39) and (40) hold between  $R_C$  and spatial infinity, SRs are the accumulation point for infalling matter starting arbitrarily far from the MCO and *regardless of its initial rotation sense* (see Fig. 1), albeit reaching the SR takes an infinite time.
- ii) This zero of  $\Omega_-$  is not continuously connected to  $R_C$  by stable timelike retrograde orbits because either (39) or (40) is violated in between. In the latter case, a stable LR exists at  $R_{LR}$  and stable timelike circular orbits exist for  $R_C < R < R_{LR}$  [24]. Thus, the LCO will tend towards the LR, albeit taking an infinite time. In the former case, the LCO will outspiral towards a radius wherein  $V'' = 0$ , delimiting a region of unstable circular orbits. Such an *outspiral plunge* signals a breakdown of the adiabaticity condition.

## 4 The quasi-circular outspiralling - concrete illustrations

Let us consider concrete MCO spacetimes where the discussed outspiralling occurs. In subsection 4.1, a simple toy model is considered, while in subsection 4.2 our focus turns to spinning BSs. In section 5, eq. (37) is solved for both these families of examples, to look for the GW signatures of such motion.

<sup>3</sup>*Mutatis mutandis* for retrograde orbits.

<sup>4</sup>This actually applies regardless of whether the approach is an inspiral or an outspiral motion. Locally, in the neighbourhood of the SR, retrograde particles inspiral to the SR, while prograde particles outspiral to the SR, under the setup above.

## 4.1 Engineered geometry

Let us construct an *ad hoc* geometry, within the symmetries discussed in section 2, with the desired geodesic behaviour. To determine the relevant functions (see eqs. (12) to (17)), it is enough to define a  $g_{tt}$  and  $g_{t\varphi}$  exclusively on the equator. The following conditions are imposed:

- i.  $g_{t\varphi} = 0 = g'_{t\varphi} = g'_{tt}$  at  $R = 0$ ;
- ii.  $g_{tt} \rightarrow -1 + \alpha/R$  and  $g_{t\varphi} \rightarrow -\beta/R$  at  $R \rightarrow \infty$ , with  $\alpha, \beta > 0$ ;
- iii. there exists  $R_C > 0$  such that  $C(R_C) = 0$ , and  $C(R) > 0$  for all  $R > R_C$ ;
- iv.  $\beta_{\pm} > 0$  and  $V_{\pm}'' < 0$ , for all  $R \geq R_C$ .

Requirement i) ensures regularity at the origin, while ii) enforces the right asymptotic behavior. Conditions iii) and iv) guarantee that the desired outspiraling orbits for the LCO are possible. Observe that iii) is verified, if  $g_{tt}$  has a local maximum between  $R_C$  and infinity.

The following parameterized choices are able to meet the requirements under appropriate choices of parameters:

$$g_{tt} = -1 + \frac{a_1 R^{k_1}}{(1+R)^{k_1+1}}, \quad g_{t\varphi} = -\frac{a_2 R^{k_2}}{(1+R)^{k_2+1}}; \quad (46)$$

for  $g_{tt}$  we choose  $a_1 = 4$  and  $k_1 = 3$ ; for  $g_{t\varphi}$  three sets of constants are chosen: a)  $a_2 = 3$  and  $k_2 = 2$ ; b)  $a_2 = 2$  and  $k_2 = 4$ ; c)  $a_2 = 0$ . With the two former choices, both  $g_{tt}$  and  $g_{t\varphi}$  have one local extremum, with case a)/b) setting the local minimum of  $g_{t\varphi}$  at a larger/lower radius than the local maximum of  $g_{tt}$  - see left panel of Fig. 2. Case c) is a spherically symmetric geometry, with  $g_{t\varphi} = 0$ .

In the spherically symmetric setting,  $R_C$  is a SR, *cf.* eq. (14). This degeneracy is lifted once  $g_{t\varphi} \neq 0$ , allowing an outspiraling region. According to Fig. 2 (right panel), in case a) the SR is retrograde with the outspiraling regime achieved if the LCO approaches the MCO via prograde orbits. In case b) the SR is prograde and thus the outspiraling occurs for initially retrograde orbits. This is a consequence of the relative position of the extrema of  $g_{tt}$  and  $g_{t\varphi}$  or, in other words, of the sign of  $g'_{t\varphi}$  at  $R_{SR}$ .

Naively, SRs could be interpreted as a balance between the LCO's angular momentum and the MCO's frame dragging [34, 35]. If true, SRs would always be retrograde, as in case a). Case b) and c), however, contradict such interpretation [60]. Nonetheless, for the spinning BSs example only retrograde SRs are found.

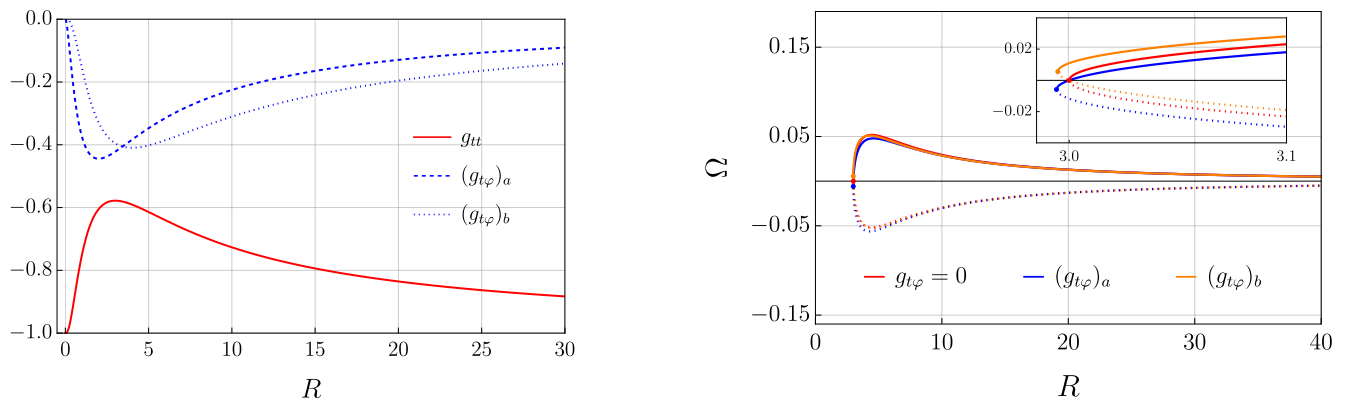


Figure 2: Toy model results. (Left) Radial profiles of  $g_{tt}$  and  $g_{t\varphi}$  in eq. (46), with the parameters defined in the text. (Right) Radial profile of  $\Omega$  for the three distinct  $g_{t\varphi}$  profiles. The continuous (dotted) lines correspond to prograde (retrograde) orbits, while the dots mark  $C = 0$ . The inset plot shows the curves zoomed near  $R = R_C$

## 4.2 Spinning boson stars

BSs are horizonless, globally regular, asymptotically flat, equilibrium solutions of the Einstein-Klein-Gordon theory with a complex massive scalar field  $\Psi$  minimally coupled to Einstein's gravity. We shall consider only mini-BSs, where no self-interactions exist. This model is described by the action

$$S = \int d^4x \sqrt{-g} \left[ \frac{\mathcal{R}}{16\pi} - g^{\alpha\beta} \partial_\alpha \Psi^* \partial_\beta \Psi - \mu^2 \Psi^* \Psi \right], \quad (47)$$

with  $\mathcal{R}$  the Ricci scalar,  $\mu$  the scalar field mass and  $\Psi^*$  the complex conjugate of  $\Psi$ . The metric ansatz considered to obtain the stationary and axisymmetric solutions reads

$$ds^2 = -e^{2F_0(r,\theta)} dt^2 + e^{2F_1(r,\theta)} (dr^2 + r^2 d\theta^2) + e^{2F_2(r,\theta)} r^2 \sin^2 \theta \left( d\varphi - \frac{W(r,\theta)}{r} dt \right)^2, \quad (48)$$

while the scalar field obeys

$$\Psi(t, r, \theta, \varphi) = \phi(r, \theta) e^{i(m\varphi - \omega t)}, \quad (49)$$

with  $\omega$  the frequency of the scalar field, and  $m = 0, \pm 1, \pm 2, \dots$  the azimuthal harmonic index with  $m = 0$  corresponding to spherically symmetric solutions. Moreover, the solutions are also labeled by the non-negative integer  $n$  associated with the number of radial nodes of  $\phi$ . The solutions considered here are characterized by  $m = 1$  and  $n = 0$  and were obtained numerically through the use of the CADSOL package [68, 69]. One important feature of these solutions is that boundary conditions, concerning the regularity of  $\Psi$  at the origin, impose that  $\phi|_{r=0} = 0$  [70]. This imposes a toroidal, off-centered distribution of the energy density. Observe that the scalar field mass  $\mu$  can be absorbed into the coordinates, by performing the substitution  $r \rightarrow r\mu$  and  $\omega \rightarrow \omega/\mu$ . Furthermore,  $\omega/\mu$  can be interpreted as a label that identifies uniquely a mini-BS, as only first branch solutions are considered.

The results for the orbital stability regions for prograde and retrograde orbits can be found in Fig. 3. The stability of the two sets of orbits differ greatly, with only retrograde orbits displaying LR and SRs. The radius of the  $C = 0$  orbit is common to both, as it is independent of the rotation sense. For these solutions, an outspiraling motion can exist exclusively for initially prograde orbits.

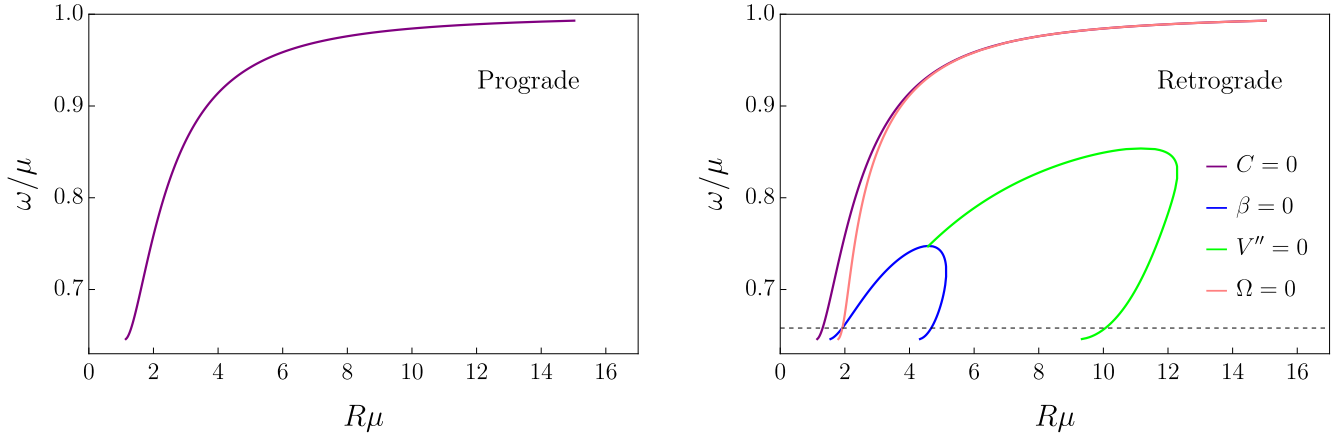


Figure 3: Structure of prograde (left) and retrograde (right) equatorial circular orbits for rotating BSs in the first branch. The black vertical dashed line, on the right panel, corresponds to  $\omega/\mu = 0.658$ , from which the endpoint switches from a SR to a stable LR.

For this class of examples, there are two outcomes for the outspiraling motion. For  $\omega/\mu > 0.658$ , the endpoint is the SR, while for  $\omega/\mu < 0.658$  the endpoint is the stable LR. For the solution with  $\omega/\mu = 0.658$  the SR coincides with the stable LR, leading to a light point orbit - Fig. 4 (left panel). This spinning BS also marks the emergence of an ergoregion, present for all solutions with  $\omega/\mu < 0.658$  [35]. Therefore, all BSs where outspiralling towards a stable LR occurs are affected by the *ergoregion instability*. Also, the stable LR, although being retrograde, will be co-rotating with the MCO for all BSs with an ergoregion. Finally, we observe there are both BSs where the maximum of the scalar field occurs at a larger and at a lower radius than both the SR and the  $C = 0$  orbits, dismissing and obvious co-relation between these quantities - Fig. 4 (right panel).

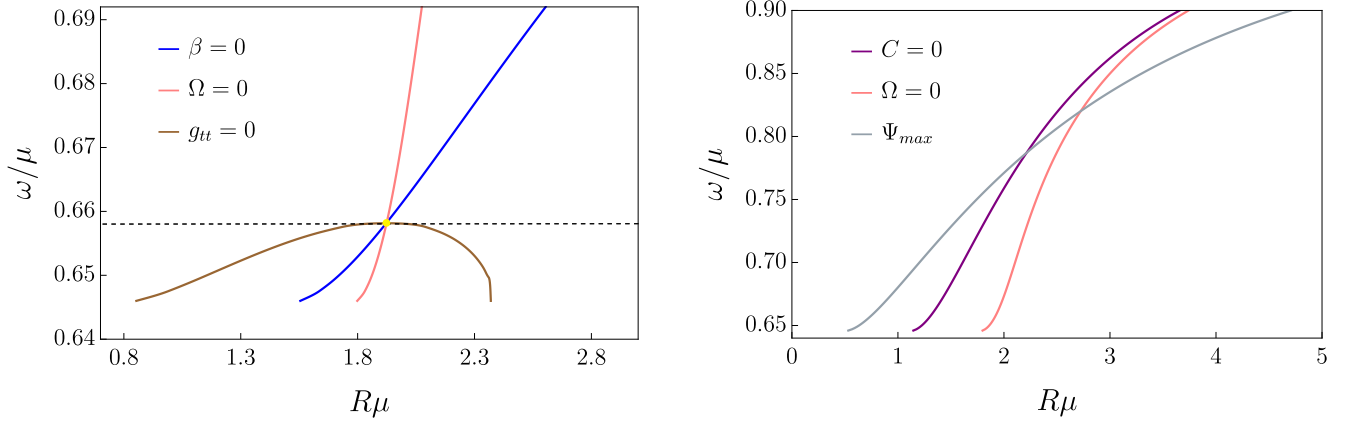


Figure 4: Properties of the rotating BSs. (Left) Emergence of ergoregion from light point orbit, where an ergosurface, a stable LR and the SR coincide. The horizontal dashed line corresponds to  $\omega/\mu = 0.658$ , with the yellow dot representing the light point orbit. (Right) Plot of the radial coordinate where  $|\Psi|$  is maximum with the SR and  $C = 0$ .

## 5 Gravitational Wave Signatures

Having laid out the theoretical description of the possible motions in generic spacetimes, and presented concrete illustrations of the outspiralling motion, it is of interest to examine possible phenomenological implications. To achieve that, we shall now solve numerically eq. (37) for the examples in section 4. As a technical point on solving this equation, due to  $dR/dt = 0$  at  $R = R_C$ , to “kick-start” the outspiral once this radius was attained from the inspiral, a perturbation was imposed taking the LCO to  $R_C + \epsilon$ . Then we obtain the GW strain as follows. In the quadrupole limit, the transverse traceless (TT) part of the metric perturbation (*i.e.* strain, assumed to be in the wave zone) at distance  $D$  is

$$h_{ij}^{TT} = \frac{2}{D} \frac{d^2 J_{ij}^{TT}}{dt^2}, \quad (50)$$

with  $J_{ij}$  the reduced quadrupole moment. Assuming the MCO is head-on with the GW detector, it holds that  $J_{ij}^{TT} = J_{ij}$ . From eqs. (34) and (35), the two gauge invariant degrees of freedom of  $h_{ij}^{TT}$ , the polarizations  $h_+$  and  $h_\times$ , are

$$h_+ = -\frac{4m}{D} R^2 \Omega^2 \cos 2\Omega t, \quad (51)$$

$$h_\times = -\frac{4m}{D} R^2 \Omega^2 \sin 2\Omega t. \quad (52)$$

In the quadrupole limit, the GW frequency is simply twice the angular velocity, *i.e.*  $f_{GW} = 2\Omega$ , and

$$\frac{h_+ D}{m} = 4R^2 \Omega^2. \quad (53)$$

Therefore, the right hand side in eq. (53) will be proportional to the strain amplitude.

### 5.1 Engineered example

We first display the results for the engineered metrics considered in subsection 4.1. The mass factor  $m$  in eq. (37) was absorbed by the dimensionful quantities:  $R$ ,  $\Omega$  and  $t$ . The initial conditions considered were  $R/m = 10$  at  $t = 0$ .

In the left panel of Fig. 5, it is displayed the outspiral behavior for spacetimes a) and b), occurring after the LCO reaches  $R_C$ , and ending towards the SR. By contrast, the spherically symmetric geometry displays only the inspiral directly towards the SR. In the right panel of Fig. 5, the angular frequency evolution is displayed. For all spacetimes, one observes a local maximum of  $|\Omega|$  occurring during the inspiral phase. This would impose a backward chirp on the emitted GWs, similar to that found in [38, 39]. This qualitative feature is a consequence of the SR endpoint. Indeed, for  $R \rightarrow +\infty$ , one must have a monotonically increasing  $|\Omega|$  as  $R$  decreases, since  $|\Omega| \sim 1/R^{3/2}$  (*cf.* eq. (24)). However, at the SR,  $|\Omega| = 0$ . Indeed, this is a clear deviation from the Keplerian intuition, as for inspirling orbits close to  $R_C$  the angular frequency does not increase monotonically with decreasing radius. Thus

$|\Omega|$  must attain a maximum at some radius and then decrease as it approaches the SR, giving rise to a backwards chirp. This is illustrated in the right panel of Fig. 2. Consequently, the backwards chirp of the radiated GWs will always occur when a transition between an inspiral and outspiral is present, with the frequency maximum occurring before the transition point. By contrast, the existence of a backwards chirp does not imply an outspiral.

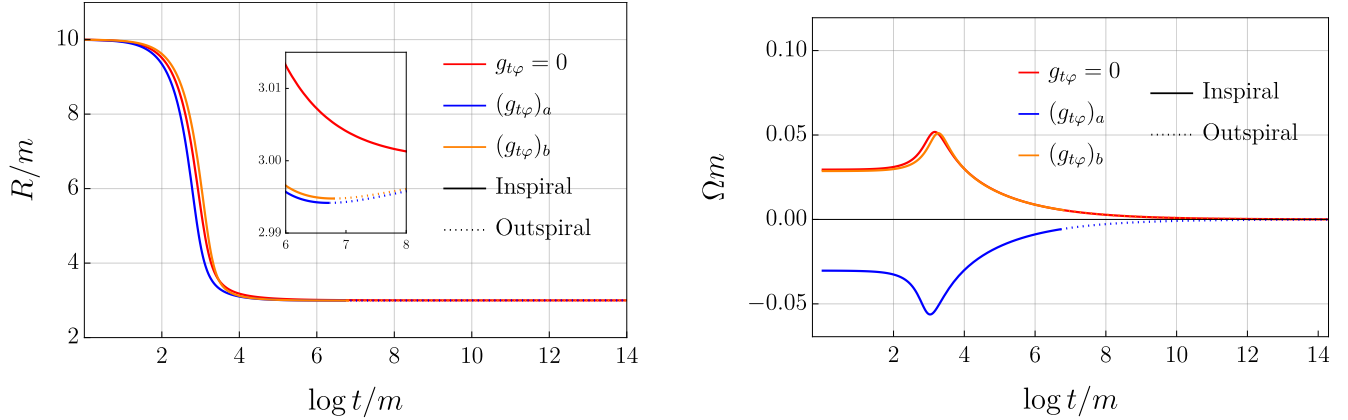


Figure 5: Evolution of  $R/m$  and  $\Omega m$  as a function of time for the engineered geometries.

Finally, in Fig. 6 the evolution of the GW strain is displayed. As the LCO approaches the SR,  $h_+ \rightarrow 0$  quadratically with  $\Omega$ . Thus, once the outspiral begins, and the frequency is already decreasing towards 0, the GW strain is already much smaller than the peak value achieved during the inspiral. These examples suggest that GW detectors may not be sensitive enough to detect radiation emitted during the outspiral, albeit a general proof is lacking.

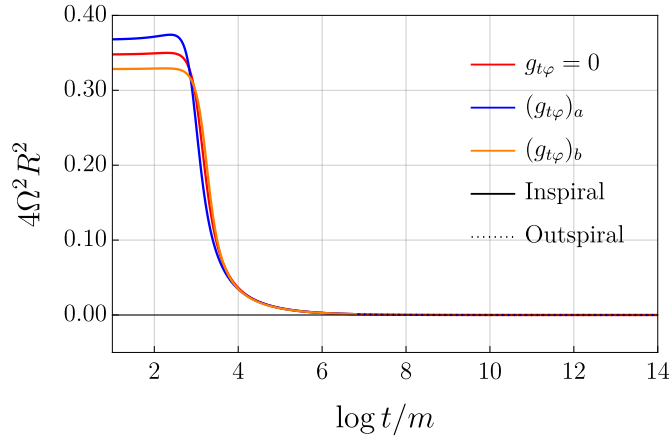


Figure 6: Evolution of  $4R^2\Omega^2 \propto h_+$  as a function of time for the engineered geometries.

## 5.2 Spinning boson stars

Let us now turn to some illustrative spinning BSs. The LCO is initially placed at a radius  $R\mu = 10$ , and the mass ratio of the system is fixed at  $m/M = 10^{-5}$ . Note that eq. (37) is invariant under the simultaneous transformation  $t \rightarrow \alpha t$  and  $m/M \rightarrow m/(\alpha M)$ . So increasing or decreasing  $m/M$ , only changes the time duration of the inspiral in this approximation, leaving its dynamics intact. Once the LCO reaches the  $C = 0$  orbit, it will start evolving according to the retrograde version of eq. (37).

The evolution was performed for rotating BSs in the first branch with  $\omega/\mu = 0.8, 0.7, 0.65$ . In Fig. 7 it is possible to see the time evolution of  $R\mu$  and the orbital angular frequency  $\Omega/\mu$  as a function of time. We see the outspiralling in the left panel and a backwards chirp in the frequency evolution in the right panel, just like in the prior subsection. The maximum of the angular frequency, once again, does not coincide with the beginning of the outspiral, occurring slightly before, which is clear from the right panel.

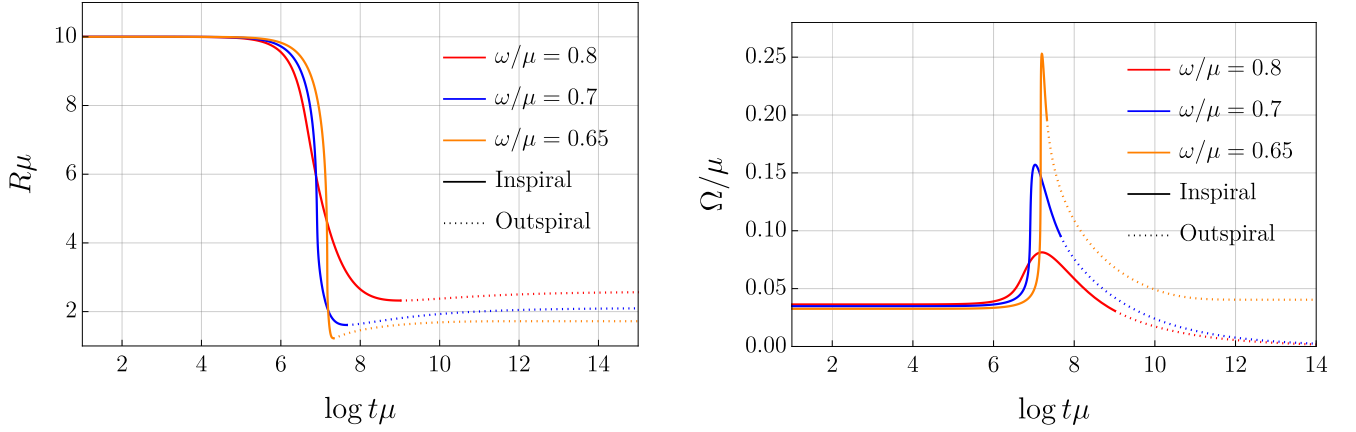


Figure 7: Evolution of  $R\mu$  and  $\Omega/\mu$  as a function of time for three distinct spinning BSs.

We can now easily observe the behaviour of the strain, from eq. (53). The right hand side of the latter equation is plotted in Fig. 8, for the three considered BSs. Due to the maximum in  $\Omega$ , the amplitude also has a local maximum during the inspiral, and is considerably suppressed in the outspiral regime. For the  $\omega/\mu = 0.65$  BS, the outspiral endpoint is a stable LR, and so neither  $\Omega/\mu$  nor  $4R^2\Omega^2$  vanish, even for large times.

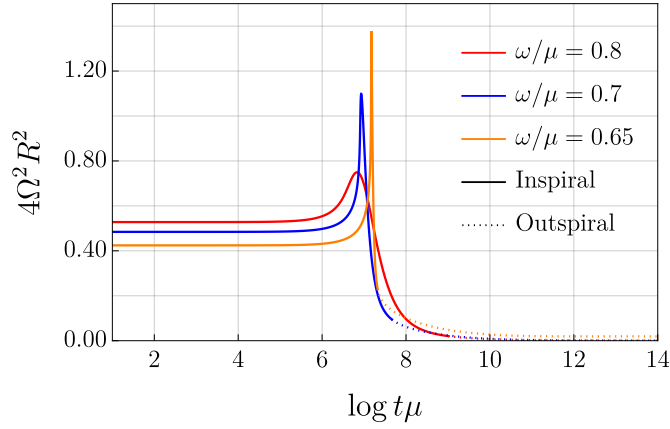


Figure 8: Evolution of  $4R^2\Omega^2 \propto h_+$  as a function of time for three distinct spinning BSs.

## 6 Conclusions and Discussions

In this work, we determined the conditions under which an object orbiting in an equatorial quasi-circular motion, can continuously transition from an inspiral to an outspiral as it loses energy adiabatically. For this to occur, it is crucial that the spacetime is spinning and that  $g_{tt}$  does not vary monotonically. By analyzing eq. (37), derived assuming the quadrupole approximation for the radiated energy of GWs, we concluded that the transition can occur at a radius where a degeneracy between prograde and retrograde orbits exists, with the LCO transitioning between the two types of orbits. Moreover, we determined that such an orbit, albeit a stationary point of eq. (37), could be reached in a finite amount of time. The outspiral endpoints could be either a SR, a stable LR, or a brief “outwards plunge” as it enters a region of unstable timelike circular orbits. We displayed a couple of examples featuring this outspiral motion: an engineered geometry and a spinning BS. The outspiral endpoint for the engineered geometry was the SR, which could occur in either the retrograde or prograde branches. For spinning BSs, even though most cases featured a SR endpoint, we found some examples where the endpoint is a stable LR, albeit being also prone to an ergoregion instability. Additionally, no co-relation between the maximum of the scalar field distribution with either the inspiral-outspiral transition radius or the SR location was found. Finally, we also calculated some GW signatures associated with the outspiral feature for both spacetimes. We concluded that a backwards chirp of the gravitational waveform was always present, even though the latter does not imply outspiralling. Indeed, the maximum of the LCO’s angular velocity (or the GW frequency, under the quadrupole approximation) occurred

before the transition. The GW strain during the outspiral motion was found to be much smaller, sometimes even negligible, relative to the maximum value.

There are a few additional remarks to be considered. Even though eq. (37) is specialized for the GW emission under the quadrupole approximation, it is expected that the outspiral motion would still occur for other energy dissipation formulae that tend to circularize orbits, i.e., that obey eq. (30). The stationary behavior at  $R_C$  does not come from the energy flux formula in eq. (36), but from the circular geodesic structure of the spacetime in eq. (32). Thus, if another energy flux would be considered, such that  $\dot{E} \neq 0$  at  $R_C$ , a transition would still be expected. We also remark that the slow rotation approximation of BSs in [71], albeit reproducing nicely the total ADM mass and angular momenta, cannot reproduce the outspiral behaviour displayed in Fig. 7. This is due to this approximation being unable to reproduce the  $C < 0$  region for the structure of circular orbits (c.f Fig. 3).

Many questions remain for future works. Firstly, it would be interesting to extend this formalism to eccentric orbits. In this case, the LCO would not “see” an infinite potential barrier at  $R_C$ , but still the dissipation would be forcing the orbits to circularize (due to eq. (30)). Additionally, we remark that the stable LR endpoint, albeit only reached at  $t \rightarrow \infty$ , appears to signal a breakdown of the formalism. At the stable LR,  $\dot{E} \neq 0$ , and thus as the LCO would approach the LR, an arbitrarily large amount of energy would be radiated via GWs, which is unphysical. Moreover, as the stable LR is being approached from inside, outwards of the stable LR, no timelike circular orbits are allowed, preventing further quasi-circular outspiral. Thus, the fate of such orbits approaching the stable LR from inwards is unclear. Finally, it would also be interesting to study the potential implications of the SR attractive nature, as accumulation points.

## 7 Acknowledgements

This work is supported by CIDMA under the FCT Multi-Annual Financing Program for R&D Units (UID/04106), through the Portuguese Foundation for Science and Technology (FCT – Fundação para a Ciência e a Tecnologia), as well as the projects: Horizon Europe staff exchange (SE) programme HORIZON-MSCA2021-SE-01 Grant No. NewFunFiCO-101086251; 2022.04560.PTDC (<https://doi.org/10.54499/2022.04560.PTDC>) and 2024.05617.CERN (<https://doi.org/10.54499/2024.05617.CERN>). M.M. is supported by the FCT grant 2024.03055.BD.

## References

- [1] B. P. Abbott et al. (LIGO Scientific, Virgo), “Observation of Gravitational Waves from a Binary Black Hole Merger”, *Phys. Rev. Lett.* **116**, 061102 (2016), arXiv:1602.03837 [gr-qc].
- [2] B. P. Abbott et al. (LIGO Scientific, Virgo), “GWTC-1: A Gravitational-Wave Transient Catalog of Compact Binary Mergers Observed by LIGO and Virgo during the First and Second Observing Runs”, *Phys. Rev. X* **9**, 031040 (2019), arXiv:1811.12907 [astro-ph.HE].
- [3] R. Abbott et al. (LIGO Scientific, Virgo), “GWTC-2: Compact Binary Coalescences Observed by LIGO and Virgo During the First Half of the Third Observing Run”, *Phys. Rev. X* **11**, 021053 (2021), arXiv:2010.14527 [gr-qc].
- [4] R. Abbott et al. (KAGRA, VIRGO, LIGO Scientific), “GWTC-3: Compact Binary Coalescences Observed by LIGO and Virgo during the Second Part of the Third Observing Run”, *Phys. Rev. X* **13**, 041039 (2023), arXiv:2111.03606 [gr-qc].
- [5] R. Abbott et al. (LIGO Scientific, VIRGO, KAGRA), “Tests of General Relativity with GWTC-3”, (2021), arXiv:2112.06861 [gr-qc].
- [6] M. Colpi et al. (LISA), “LISA Definition Study Report”, (2024), arXiv:2402.07571 [astro-ph.CO].
- [7] P. A. Seoane et al. (LISA), “Astrophysics with the Laser Interferometer Space Antenna”, *Living Rev. Rel.* **26**, 2 (2023), arXiv:2203.06016 [gr-qc].
- [8] P. Auclair et al. (LISA Cosmology Working Group), “Cosmology with the Laser Interferometer Space Antenna”, *Living Rev. Rel.* **26**, 5 (2023), arXiv:2204.05434 [astro-ph.CO].
- [9] K. G. Arun et al. (LISA), “New horizons for fundamental physics with LISA”, *Living Rev. Rel.* **25**, 4 (2022), arXiv:2205.01597 [gr-qc].
- [10] C. Caprini, A. Heffernan, R. Brito, G. Franciolini, G. Nardini, N. Tamanini, and D. Steer, “Science of the LISA mission: A Summary for the European Strategy for Particle Physics”, (2025), arXiv:2507.05130 [gr-qc].

- [11] B. Carter, “Axisymmetric black hole has only two degrees of freedom”, *Phys. Rev. Lett.* **26**, 331–333 (1971).
- [12] D. C. Robinson, “Uniqueness of the Kerr black hole”, *Phys. Rev. Lett.* **34**, 905–906 (1975).
- [13] P. T. Chrusciel, J. Lopes Costa, and M. Heusler, “Stationary Black Holes: Uniqueness and Beyond”, *Living Rev. Rel.* **15**, 7 (2012), arXiv:1205.6112 [gr-qc].
- [14] C. A. R. Herdeiro, “Black Holes: On the Universality of the Kerr Hypothesis”, *Lect. Notes Phys.* **1017**, 315–331 (2023), arXiv:2204.05640 [gr-qc].
- [15] V. Cardoso and P. Pani, “Testing the nature of dark compact objects: a status report”, *Living Rev. Rel.* **22**, 4 (2019), arXiv:1904.05363 [gr-qc].
- [16] D. C. Wilkins, “Bound Geodesics in the Kerr Metric”, *Phys. Rev. D* **5**, 814–822 (1972).
- [17] S. Chandrasekhar, *The mathematical theory of black holes* (1985).
- [18] V. Diemer, K. Eilers, B. Hartmann, I. Schaffer, and C. Toma, “Geodesic motion in the space-time of a noncompact boson star”, *Phys. Rev. D* **88**, 044025 (2013), arXiv:1304.5646 [gr-qc].
- [19] P. Grandclement, C. Somé, and E. Gourgoulhon, “Models of rotating boson stars and geodesics around them: new type of orbits”, *Phys. Rev. D* **90**, 024068 (2014), arXiv:1405.4837 [gr-qc].
- [20] M. Groud, Z. Meliani, F. H. Vincent, P. Grandclément, and E. Gourgoulhon, “Comparing timelike geodesics around a Kerr black hole and a boson star”, *Class. Quant. Grav.* **34**, 215007 (2017), arXiv:1709.05938 [astro-ph.HE].
- [21] K. Glampedakis and G. Pappas, “Modification of photon trapping orbits as a diagnostic of non-Kerr spacetimes”, *Phys. Rev. D* **99**, 124041 (2019), arXiv:1806.09333 [gr-qc].
- [22] F. Bacchini, D. R. Mayerson, B. Ripperda, J. Davelaar, H. Olivares, T. Hertog, and B. Vercoocke, “Fuzzball Shadows: Emergent Horizons from Microstructure”, *Phys. Rev. Lett.* **127**, 171601 (2021), arXiv:2103.12075 [hep-th].
- [23] L. G. Collodel, D. D. Doneva, and S. S. Yazadjiev, “Circular Orbit Structure and Thin Accretion Disks around Kerr Black Holes with Scalar Hair”, *Astrophys. J.* **910**, 52 (2021), arXiv:2101.05073 [astro-ph.HE].
- [24] J. F. M. Delgado, C. A. R. Herdeiro, and E. Radu, “Equatorial timelike circular orbits around generic ultra-compact objects”, *Phys. Rev. D* **105**, 064026 (2022), arXiv:2107.03404 [gr-qc].
- [25] K. Destounis, A. G. Suvorov, and K. D. Kokkotas, “Gravitational-wave glitches in chaotic extreme-mass-ratio inspirals”, *Phys. Rev. Lett.* **126**, 141102 (2021), arXiv:2103.05643 [gr-qc].
- [26] Y.-P. Zhang, Y.-B. Zeng, Y.-Q. Wang, S.-W. Wei, and Y.-X. Liu, “Motion of test particle in rotating boson star”, *Phys. Rev. D* **105**, 044021 (2022), arXiv:2107.04848 [gr-qc].
- [27] Y.-P. Zhang, Y.-B. Zeng, Y.-Q. Wang, S.-W. Wei, and Y.-X. Liu, “Equatorial orbits of spinning test particles in rotating boson stars”, *Eur. Phys. J. C* **82**, 809 (2022), arXiv:2201.01498 [gr-qc].
- [28] A. M. Pombo and I. D. Saltas, “A Sun-like star orbiting a boson star”, *Mon. Not. Roy. Astron. Soc.* **524**, 4083–4090 (2023), arXiv:2304.09140 [astro-ph.SR].
- [29] J. L. Rosa, D. S. J. Cordeiro, C. F. B. Macedo, and F. S. N. Lobo, “Observational imprints of gravastars from accretion disks and hot spots”, *Phys. Rev. D* **109**, 084002 (2024), arXiv:2401.07766 [gr-qc].
- [30] I. Sengo, P. V. P. Cunha, C. A. R. Herdeiro, and E. Radu, “The imitation game reloaded: effective shadows of dynamically robust spinning Proca stars”, *JCAP* **05**, 054 (2024), arXiv:2402.14919 [gr-qc].
- [31] R. Torres, “Observational and theoretical aspects of superspinars”, *Gen. Rel. Grav.* **57**, 50 (2025), arXiv:2407.14851 [gr-qc].
- [32] K. Gjorgjieski, J. Kunz, and P. Nedkova, “Circular Orbits and Photon Orbits at Wormhole Throats”, (2025), arXiv:2505.07507 [gr-qc].
- [33] B. Bermúdez-Cárdenas and O. Lasso Andino, “Light rings, timelike circular orbits and curvature of traversable wormholes”, (2025), arXiv:2504.10732 [gr-qc].
- [34] L. G. Collodel, B. Kleihaus, and J. Kunz, “Static Orbits in Rotating Spacetimes”, *Phys. Rev. Lett.* **120**, 201103 (2018), arXiv:1711.05191 [gr-qc].
- [35] P. Grandclément, “Light rings and light points of boson stars”, *Phys. Rev. D* **95**, 084011 (2017), arXiv:1612.07507 [gr-qc].

- [36] T. A. Apostolatos, G. Lukes-Gerakopoulos, and G. Contopoulos, “How to Observe a Non-Kerr Spacetime Using Gravitational Waves”, *Phys. Rev. Lett.* **103**, 111101 (2009), arXiv:0906.0093 [gr-qc].
- [37] M. Kesden, J. Gair, and M. Kamionkowski, “Gravitational-wave signature of an inspiral into a supermassive horizonless object”, *Phys. Rev. D* **71**, 044015 (2005), arXiv:astro-ph/0411478.
- [38] J. F. M. Delgado, C. A. R. Herdeiro, and E. Radu, “EMRIs around  $j = 1$  black holes with synchronised hair”, *JCAP* **10**, 029 (2023), arXiv:2305.02333 [gr-qc].
- [39] L. G. Collodel, D. D. Doneva, and S. S. Yazadjiev, “Equatorial extreme-mass-ratio inspirals in Kerr black holes with scalar hair spacetimes”, *Phys. Rev. D* **105**, 044036 (2022), arXiv:2108.11658 [gr-qc].
- [40] M. C. Teodoro, L. G. Collodel, and J. Kunz, “Retrograde Polish Doughnuts around Boson Stars”, *JCAP* **03**, 063 (2021), arXiv:2011.10288 [gr-qc].
- [41] M. C. Teodoro, L. G. Collodel, D. Doneva, J. Kunz, P. Nedkova, and S. Yazadjiev, “Thick toroidal configurations around scalarized Kerr black holes”, *Phys. Rev. D* **104**, 124047 (2021), arXiv:2108.08640 [gr-qc].
- [42] K. Destounis, F. Angeloni, M. Vaglio, and P. Pani, “Extreme-mass-ratio inspirals into rotating boson stars: Nonintegrability, chaos, and transient resonances”, *Phys. Rev. D* **108**, 084062 (2023), arXiv:2305.05691 [gr-qc].
- [43] A. Cipriani, A. De Santis, G. Di Russo, A. Grillo, and L. Tabarroni, “Hamiltonian Neural Networks approach to fuzball geodesics”, (2025), arXiv:2502.20881 [hep-th].
- [44] K. Glampedakis, S. A. Hughes, and D. Kennefick, “Approximating the inspiral of test bodies into Kerr black holes”, *Phys. Rev. D* **66**, 064005 (2002), arXiv:gr-qc/0205033.
- [45] S. A. Hughes, “Evolution of circular, nonequatorial orbits of Kerr black holes due to gravitational wave emission. II. Inspiral trajectories and gravitational wave forms”, *Phys. Rev. D* **64**, [Erratum: *Phys.Rev.D* 88, 109902 (2013)], 064004 (2001), arXiv:gr-qc/0104041.
- [46] J. R. Gair, D. J. Kennefick, and S. L. Larson, “Semi-relativistic approximation to gravitational radiation from encounters with black holes”, *Phys. Rev. D* **72**, [Erratum: *Phys.Rev.D* 74, 109901 (2006)], 084009 (2005), arXiv:gr-qc/0508049.
- [47] K. Glampedakis and D. Kennefick, “Zoom and whirl: Eccentric equatorial orbits around spinning black holes and their evolution under gravitational radiation reaction”, *Phys. Rev. D* **66**, 044002 (2002), arXiv:gr-qc/0203086.
- [48] E. Poisson, A. Pound, and I. Vega, “The Motion of point particles in curved spacetime”, *Living Rev. Rel.* **14**, 7 (2011), arXiv:1102.0529 [gr-qc].
- [49] P. Amaro-Seoane, J. R. Gair, M. Freitag, M. Coleman Miller, I. Mandel, C. J. Cutler, and S. Babak, “Astrophysics, detection and science applications of intermediate- and extreme mass-ratio inspirals”, *Class. Quant. Grav.* **24**, R113–R169 (2007), arXiv:astro-ph/0703495.
- [50] S. Babak, J. Gair, A. Sesana, E. Barausse, C. F. Sopuerta, C. P. L. Berry, E. Berti, P. Amaro-Seoane, A. Petiteau, and A. Klein, “Science with the space-based interferometer LISA. V: Extreme mass-ratio inspirals”, *Phys. Rev. D* **95**, 103012 (2017), arXiv:1703.09722 [gr-qc].
- [51] C. P. L. Berry, S. A. Hughes, C. F. Sopuerta, A. J. K. Chua, A. Heffernan, K. Holley-Bockelmann, D. P. Mihaylov, M. C. Miller, and A. Sesana, “The unique potential of extreme mass-ratio inspirals for gravitational-wave astronomy”, *Bull. Am. Astron. Soc.* **51**, 42 (2019), arXiv:1903.03686 [astro-ph.HE].
- [52] A. Cárdenas-Avendaño and C. F. Sopuerta, “Testing gravity with extreme-mass-ratio inspirals”, in *Recent progress on gravity tests: challenges and future perspectives*, edited by C. Bambi and A. Cárdenas-Avendaño (Springer Nature Singapore, Singapore, 2024), pp. 275–359, arXiv:2401.08085 [gr-qc].
- [53] C. A. R. Herdeiro and E. Radu, “Kerr black holes with scalar hair”, *Phys. Rev. Lett.* **112**, 221101 (2014), arXiv:1403.2757 [gr-qc].
- [54] C. Herdeiro and E. Radu, “Construction and physical properties of Kerr black holes with scalar hair”, *Class. Quant. Grav.* **32**, 144001 (2015), arXiv:1501.04319 [gr-qc].
- [55] C. A. R. Herdeiro and E. Radu, “Asymptotically flat black holes with scalar hair: a review”, *Int. J. Mod. Phys. D* **24**, edited by C. A. R. Herdeiro, V. Cardoso, J. P. S. Lemos, and F. C. Mena, 1542014 (2015), arXiv:1504.08209 [gr-qc].
- [56] R. Brito, V. Cardoso, and P. Pani, “Superradiance: New Frontiers in Black Hole Physics”, *Lect. Notes Phys.* **906**, pp.1–237 (2015), arXiv:1501.06570 [gr-qc].

- [57] W. E. East and F. Pretorius, “Superradiant Instability and Backreaction of Massive Vector Fields around Kerr Black Holes”, *Phys. Rev. Lett.* **119**, 041101 (2017), arXiv:1704.04791 [gr-qc].
- [58] C. A. R. Herdeiro and E. Radu, “Dynamical Formation of Kerr Black Holes with Synchronized Hair: An Analytic Model”, *Phys. Rev. Lett.* **119**, 261101 (2017), arXiv:1706.06597 [gr-qc].
- [59] C. Herdeiro and E. Radu, “Ergosurfaces for Kerr black holes with scalar hair”, *Phys. Rev. D* **89**, 124018 (2014), arXiv:1406.1225 [gr-qc].
- [60] A. Lehébel and V. Cardoso, “Fate of observers in circular motion”, *Phys. Rev. D* **105**, 064014 (2022), arXiv:2202.08850 [gr-qc].
- [61] B. Carter, “The commutation property of a stationary, axisymmetric system”, *Commun. Math. Phys.* **17**, 233–238 (1970).
- [62] R. M. Wald, *General Relativity* (Chicago Univ. Pr., Chicago, USA, 1984).
- [63] K. Van Aelst, “Note on equatorial geodesics in circular spacetimes”, *Class. Quant. Grav.* **37**, 207001 (2020), arXiv:2103.01816 [gr-qc].
- [64] R. W. D. Nickalls, “Viète, descartes and the cubic equation”, *The Mathematical Gazette* **90**, 203–208 (2006).
- [65] V. Cardoso, C. F. B. Macedo, and R. Vicente, “Eccentricity evolution of compact binaries and applications to gravitational-wave physics”, *Phys. Rev. D* **103**, 023015 (2021), arXiv:2010.15151 [gr-qc].
- [66] P. V. P. Cunha, E. Berti, and C. A. R. Herdeiro, “Light-Ring Stability for Ultracompact Objects”, *Phys. Rev. Lett.* **119**, 251102 (2017), arXiv:1708.04211 [gr-qc].
- [67] P. V. P. Cunha and C. A. R. Herdeiro, “Stationary black holes and light rings”, *Phys. Rev. Lett.* **124**, 181101 (2020), arXiv:2003.06445 [gr-qc].
- [68] W. Schönauer and E. Schnepf, “Fidisol: a ‘black box’ solver for partial differential equations”, *Parallel Computing* **6**, 185–193 (1988).
- [69] W. Schönauer and T. Adolph, “How we solve pdes”, *Journal of Computational and Applied Mathematics* **131**, 473–492 (2001).
- [70] B. Kleihaus, J. Kunz, M. List, and I. Schaffer, “Rotating Boson Stars and Q-Balls. II. Negative Parity and Ergoregions”, *Phys. Rev. D* **77**, 064025 (2008), arXiv:0712.3742 [gr-qc].
- [71] J. F. M. Delgado, J. C. Degollado, L. E. Martínez, and M. Salgado, “Slowly Rotating Boson Stars”, (2024), arXiv:2408.05262 [gr-qc].